

1 **Integrating underwater video into traditional fisheries indices using a hierarchical**  
2 **formulation of a state-space model**

3

4 Daniel C. Gwinn<sup>a,b\*</sup>, Nathan M. Bacheler<sup>c</sup> and Kyle Shertzer<sup>c</sup>

5

6 <sup>a</sup> Biometric Research, 3 Hulbert Street, South Fremantle 6162, Western Australia, Australia.

7 <sup>b</sup> The University of Western Australia, School of Biological Sciences, Perth, Western  
8 Australia, Australia.

9 <sup>c</sup> National Marine Fisheries Service, Southeast Fisheries Science Center, Beaufort, North  
10 Carolina, United States of America.

11

12 \*Corresponding author: Daniel C. Gwinn, [dgwinnbr@gmail.com](mailto:dgwinnbr@gmail.com)

13

14 **Abstract**

15 Indices of abundance are commonly used in fisheries stock assessment models to  
16 represent trends in population size over time; however, an index can misrepresent such trends  
17 when catchability varies, sampling gears change or spatial sampling frames shift. Here we  
18 develop a state-space model in a Bayesian framework that combines both chevron trap  
19 catches and video counts into a single integrated index. The modeling approach accounts for  
20 variation in sampling efficiency (catchability) of both sampling gears and adjusts for aspects  
21 of changes in the spatial sampling frame (sampling intensity and spatial coverage) through  
22 time due to monitoring program development. We validate the model using a simulation  
23 study and then demonstrate its utility using data on vermilion snapper *Rhomboplites*  
24 *aurorubens* from the period 1990-2016. The index suggests high variation in the abundance  
25 of vermilion snapper, particularly for years previous to 2000 and a systematic decline in

26 abundance between the early 1990s and 2016. This pattern culminates (2016) with vermilion  
27 snapper at about 16% of their average early 1990s abundance which is a stronger decline than  
28 is indicated by the current index used for stock assessment of the species.

29

30 **Keywords:** Vermilion snapper, abundance index, Bayesian model, catchability

31

32

## 33 1. Introduction

34

35 Fisheries harvest policies are typically based on the results of fitting population  
36 dynamics models with a variety of data types (Hilborn and Walters, 1992; Walters and  
37 Martell, 2004). One essential piece of information used in many fisheries stock assessments  
38 is a metric that indexes changes in total stock size through time (Maunder and Punt, 2004).  
39 These indices are typically derived from some form of fishery-dependent or -independent  
40 catch or count per-unit-effort data and are assumed to change in proportion to abundance, and  
41 thus reflect a scaled version of the total stock size. The resultant indices are used to “tune”  
42 stock assessment models, affecting estimates of population dynamics quantities and  
43 management reference points, such as harvest targets. Due to their importance for effective  
44 fisheries management, much attention has been paid to fisheries index development (e.g.  
45 Maunder and Starr, 2003; Maunder and Punt, 2004; Maunder et al., 2006); however,  
46 obtaining efficacious indices reflecting true changes in total stock size can be quite difficult  
47 (Kimura and Somerton, 2006).

48 Analysts face many challenges when developing abundance indices for stock  
49 assessments, particularly regarding the assumption of proportionality. One of the simplest  
50 representations of an abundance index is  $I_t = N_t q$ , where the index  $I_t$  is the product of the  
51 true abundance  $N_t$  and the catchability  $q$  (i.e. the proportion of  $N_t$  sampled). As long as  
52 catchability is constant through time, the assumption of proportionality is met and the index  
53 will have the desirable property of reflecting true proportional changes in abundance.  
54 However, when catchability varies, changes in  $q$  (or  $q_t$ ) are confounded with changes in  $N_t$ ,  
55 such that  $I_t$  may not adequately represent true abundance trends. Complicating this matter is  
56 that  $q$  (almost) always varies when sampling fish for a variety of reasons (Monk, 2013;  
57 Gwinn et al., 2016). For example, the influence of vessel effects on catchability and fishery-

58 dependent indices is well known with variation in  $q$  related to variables such as vessel size,  
59 crew size, GPS technology, power of motor, and specific gear characteristics (Maunder,  
60 2001; Maunder and Punt, 2004; Thorson and Ward, 2014). Fisheries-independent data for use  
61 in developing abundance indices are generally recognized as superior to fishery-dependent  
62 data (e.g. Dennis et al., 2015), however, these data are similarly vulnerable to variable  $q$ . For  
63 example, the catchability of reef fish with common baited traps can be strongly related to  
64 environmental variables such as temperature, depth, soak time, and substrate characteristics  
65 (Coggins et al., 2014; Bacheler et al., 2014; Shertzer et al., 2016). At best, these influences on  
66 catchability add noise into catch data but can also result in spurious patterns in  $I_t$  that do not  
67 reflect  $N_t$  when influential variables change systematically across space and time (e.g.  
68 Walters and Maguire, 1996; Ward, 2008; Langseth et al., 2016).

69         Shifts in sampling design elements such as the spatial frame of sampling and  
70 sampling methods commonly occur in long-term monitoring programs. Typically intended to  
71 improve sampling, these idiosyncrasies can also create challenges when developing fisheries  
72 indices (Conn et al., 2017). Similar to changes in catchability, changes in the spatial sampling  
73 frame and associated environmental characteristics can influence the component of the stock  
74 targeted by sampling (e.g. Walters and Maguire, 1996; Langseth et al., 2016). This is also  
75 true for changes in sampling gears and is the reason why there is a continuous development  
76 of methods to create spatially-explicit indices (e.g. Walters, 2003; Cao et al., 2017;  
77 Ducharme-Barth et al., 2018) and indices that integrate multiple sampling methods (e.g.  
78 Conn, 2010; Gibson-Reinemer et al., 2017; Kotwicki et al., 2018; Ono et al., 2018). Thus,  
79 methods that are robust to variation in catchability due to environmental variables, as well as  
80 shifts in sampling frame and sampling methods, are important tools for stock assessment  
81 scientists (Maunder and Piner, 2015).

82           The management of many economically important reef fisheries along the southeast  
83 U.S. Atlantic coast rely on indices derived from surveys using fishery-independent chevron  
84 traps. These traps have been used in this region since 1990 but were fitted with video cameras  
85 beginning in 2011 to further understand the quality of chevron trap catch data for indexing  
86 reef fish abundance, including species that do not enter traps (Bacheler et al., 2013a; Shertzer  
87 et al., 2016). The use of underwater video to assess the properties of various sampling gears  
88 is becoming increasingly common in the literature (e.g. Ward, 2008; Parker et al., 2016;  
89 Streich et al., 2018) and can result in a form of replicated count data that may be used to  
90 index abundance (Bacheler et al., 2013b; Schonbernd et al., 2014). However, appropriate  
91 statistical methods that create indices from data collected with these two sampling gears have  
92 yet to be developed. Combining data from multiple gears presents the opportunity for  
93 improved inference, but in this case, introduces two prominent challenges. Firstly, the paired  
94 samples of the chevron trap and video count are not fully independent. Although each gear  
95 represents an independent sample of the vulnerable fish community at the survey location,  
96 they are non-independent at the spatial scale of inference (i.e. the region) because samples are  
97 collected from the same locations and thus do not represent two independent measures of  
98 stock size at the regional level. Secondly, early research comparing trap catches to video  
99 counts revealed substantial variation between the two (Bacheler et al., 2013b), likely due to  
100 differences in how environmental conditions influenced the catchability of traps and videos  
101 for various species of fish (Bacheler et al., 2014; Coggins et al., 2014).

102           Here we develop a novel fishery-independent index of abundance that integrates  
103 paired trap catches and video counts into a single index of stock size using a Bayesian  
104 hierarchical formulation of a state-space model (SSM). The SSM has three key features that  
105 make it potentially useful for this application: (i) The model incorporates the baited trap  
106 catches and video counts into a single index that accounts for dependence between the gears;

107 (ii) the model accommodates changes in catchability due to temporal and spatial variation in  
108 the environment through the use of covariates and random effects of the observation  
109 processes; and (iii) the model can account for aspects of variable catchability due to shifts in  
110 the sampling frame by modeling temporal variation at the meta-population scale separate  
111 from spatial variation at the sub-population scale. We apply this model to vermilion snapper  
112 (*Rhomboplites aurorubens*) data collected along the southeast U.S. Atlantic coast by the  
113 Southeast Reef Fish Survey as an example and compare it to an index developed with the  
114 current methods (Conn, 2010) taken from the most recent stock assessment for the species  
115 (SEDAR, 2018). The current method of index development (i.e. Conn, 2010) treats the  
116 chevron trap catches and camera counts as independent measures of the stock and does not  
117 explicitly account for shifts in the spatial frame of the surveys, thus offering a useful  
118 comparison for the SSM method.

119

## 120 **2. Methods**

121

### 122 *2.1 Overview of methods*

123

124 We organize our methods in four main parts. First, we describe the sampling design  
125 and data treatment in the context of the Southeast Reef Fish Survey sampling of *R.*  
126 *aurorubens* along the southeastern coast of the U.S., which is the motivation behind our  
127 model; second, we describe the general model structure, covariate structure, model fit  
128 evaluation and model optimization methods used in the example analyses; third we describe  
129 how we compare our index to the current index used for stock assessment of *R. aurorubens*;  
130 and last we describe validation methods of our model on a set of simplified simulated data  
131 sets.

132  
133  
134  
135  
136  
137  
138  
139  
140  
141  
142  
143  
144  
145  
146  
147  
148  
149  
150  
151  
152  
153  
154  
155  
156

## 2.2 Sampling design

*R. aurorubens* count data were collected along the southeast United States Atlantic Coast from Florida to North Carolina by the Southeast Reef Fish Survey (Fig. 1a). All baited traps were set on or near hard-bottom reef locations. There were 15,629 chevron trap samples available covering a period of 27 years (1990-2016). The number of locations sampled has varied substantially among years due to program development and funding. In the early years, the number of samples collected annually was typically in the range of several hundred; however, this number has expanded severalfold to over thirteen hundred in the most recent years. Along with increased sampling intensity, the sampling frame of the program has expanded in both the latitudinal and longitudinal directions, thus shifting the sub component of the stock vulnerable to sampling (for a detailed description of the sampling frame shift, see Appendix A). Traps were set no closer than 200 m from one another to maintain spatial independence relative to fish movement, and at depths between 13 and 115 m. All trap sites used for this analysis were selected randomly from a defined sampling frame of hard-bottom sampling points (Bacheler et al., 2014). Traps were baited with menhaden and set for approximately 90 min. For the time period of 2011-2016, the chevron traps were fitted with an outward-looking video camera (Fig. 1b) resulting in 7,644 41-frame video samples (Fig. 1c). The camera (Canon Vixia HFS200 in 2011 - 2014 and GoPro Hero 3 or 4 in 2015 and 2016) recorded at least 20 minutes of video from the bottom, and videos were read according to Schobernd et al. (2014). Specifically, a series of video frames spaced 30 seconds apart were read 10 to 30 minutes after the trap landed on the bottom. This resulted in 41 replicate camera samples and one baited trap sample per site.

157 2.3 *Data and treatment*

158

159 For trap data, we analyzed the un-transformed catch and for the video data, the sum of  
160 the counts across the 41 camera frames (*SumCount*). We chose to use the *SumCount* of the  
161 camera data because *SumCount* changes linearly with the *MeanCount* (Bacheler and  
162 Carmichael, 2014), which is often the preferred camera metric (Conn, 2011; Schobernd et al.,  
163 2014; Campbell et al., 2015), and using the *SumCount* preserves the discrete nature of the  
164 camera counts allowing for the use of derivations of the Poisson distribution to describe both  
165 the chevron trap and camera observation processes. We applied several data filters to either  
166 simplify predictor variables, remove records with missing predictor variables, or to remove  
167 unusual values. Detailed methods of the data cleaning process are reported in Appendix B.

168

169 2.4 *Model development*

170

171 The model was formulated with three distinct hierarchical layers such that the relative  
172 abundance at the meta-population level (representing our index of interest, denoted as  $I_t$ ) was  
173 modeled separately from the relative abundance at the sub-population level (i.e. at sample  
174 sites, denoted as  $n_{s,t}$ ) and separately from the observation processes. By modelling the meta-  
175 population level abundance separately from the sub-population abundance, we were able to  
176 isolate the fishery index of interest from components of spatial variation among sampling  
177 locations. This is the key component that separates shifts in spatial sampling frame relative to  
178 latitude, longitude, and depth from the changes in the average meta-population abundance.  
179 Furthermore, by modeling the abundance processes and observation processes with separate  
180 sub-models we were able to separate observation error from process error and account for  
181 systematic variation in catchability.



182 The most general version of our model describes the latent meta-population level  
 183 relative abundance (hereafter referred to simply as abundance,  $I_t$ ) for each year as an  
 184 independent, freely estimated parameter represented as:

$$\log I_t \sim \text{Normal}(0, 100) \quad (1)$$

186  
 187 however more constrained formulations that assume that meta-population level abundance is  
 188 a random effect among years (i.e.  $\log I_t \sim \text{Normal}(\bar{I}, \sigma)$ ), a Markovian random walk (i.e.  
 189  $\log I_t = \log I_{t-1} + r_t$ , where  $r_t \sim \text{Normal}(\bar{r}, \sigma)$ ), or any population dynamics model (e.g.  
 190 logistic model, age-structured model) could be applied based on the intended use of the  
 191 index. If the index will be used to fit a more complex population dynamics model for stock  
 192 assessment, it may be desirable to impose as little constraint on the temporal pattern of the  
 193 index as possible; thus, we present the model that assumes indexes are independence among  
 194 years to represent this case.

195 Spatial variation in abundance across sample sites each year (sub-population level)  
 196 was modeled on the log scale as:

$$\log(n_{s,t}) = \log I_t + \text{CO}_{s,t}^n + \varepsilon_{s,t}^{abun} \quad (2)$$

198  
 199 where the term  $\log I_t$  is the year specific intercept of the linear model,  $\text{CO}_{s,t}^n$  is a linear  
 200 combination of spatial covariates, and  $\varepsilon_{s,t}^{abun}$  describes random site-level variation in  
 201 abundance that is not explained by the covariate structure.

202 We approximated the baited trap catches ( $c_{s,t}^{trap}$ ) and the camera *SumCounts* ( $c_{s,t}^{cam}$ ) as  
 203 deviates drawn from Poisson log-Normal distributions, which are similar in character to  
 204 negative binomial distributions (Ntzoufras, 2009, p. 315-317), but can demonstrate better

205 mixing properties than negative binomial distributions when applied in Bayesian programs  
 206 such as JAGS. We specified these models as:

207

$$c_{s,t}^{trap} \sim \text{Poisson} \left( e^{\log(n_{s,t}) + cov_{s,t}^{trap} + \varepsilon_{s,t}^{trap}} \right) \quad (3)$$

$$c_{s,t}^{cam} \sim \text{Poisson} \left( e^{\log(n_{s,t}) + cov_{s,t}^{cam} + \varepsilon_{s,t}^{cam}} \right) \quad (4)$$

208

209 where the mean on the log scale is the site-specific abundance  $n_{s,t}$  plus a linear combination  
 210 of environmental and/or sampling covariates (i.e.  $co_{t,j}^{trap}$  and  $co_{t,j}^{cam}$ ) to account for  
 211 systematic variation in catchability. The parameters  $\varepsilon_{s,t}^{trap}$  and  $\varepsilon_{s,t}^{cam}$  are gear-specific log-  
 212 Normal distributed random observation errors modeled as,  $\varepsilon_{s,t} \sim \text{Normal} \left( 0, \sigma \right)$ , with a mean  
 213 of zero and an estimated standard deviation specific to each sampling method (i.e.  $\sigma^{trap}$  and  
 214  $\sigma^{cam}$ ).

215

## 216 2.5 Model covariates

217

218 To account for systematic variation in our count data, we incorporated a suite of  
 219 covariates into the abundance and observation sub-models. We selected covariates based on  
 220 two key considerations. Our first consideration was to separate covariates that influenced the  
 221 spatial distribution of fish from those that influenced temporal patterns in fish abundance.  
 222 This was important because spatial and temporal patterns of abundance are modeled in two  
 223 separate hierarchical layers (i.e. equation 1 and 2) to create a distinction between the fishery  
 224 index, i.e. temporal patterns in abundance at the meta-population level ( $I_t$ ), from spatial  
 225 variation in the data due to patterns in the spatial distribution of fish ( $n_{s,t}$ ) and shifts in the  
 226 sampling frame through time. Thus, we included nonlinear (quadratic) effects of latitude ( $lat$

227 and  $lat^2$ ), longitude ( $lon$  and  $lon^2$ ) and depth ( $dep$  and  $dep^2$ ), as well as the potential  
 228 interaction between latitude and longitude as covariates of local-scale abundance. We  
 229 included both main and quadratic effects of these variables to account for any optimal ranges  
 230 in latitude, longitude and depth within our sampling frame that vermilion snapper may prefer.  
 231 The interaction between latitude and longitude was included to allow any preferred range of  
 232 one variable to be dependent on the other. For example, if vermilion snapper demonstrated a  
 233 preferred distance from shore, a positive interaction between latitude and longitude could  
 234 approximate this spatial distribution. Lastly, we included a measure of bottom relief ( $rel$ ) and  
 235 the percent of the substrate that was hard-bottom ( $sub$ ) as these habitat features may affect the  
 236 local density of fish. Spatial covariates of abundance were incorporated into the model as:

$$237 \quad co_{s,t}^n = \beta_1 lat_{s,t} + \beta_2 lat_{s,t}^2 + \beta_3 dep_{s,t} + \beta_4 dep_{s,t}^2 + \beta_5 lon_{s,t} + \beta_6 lon_{s,t}^2 + \quad (5)$$

$$\beta_7 lat_{s,t} lon_{s,t} + \beta_8 rel_{s,t} + \beta_9 sub_{s,t}.$$

238

239 Our second key consideration was to separate covariates of the abundance and  
 240 observation processes. This was important because our model likely has limited ability to  
 241 disentangle systematic patterns in abundance from systematic patterns in catchability when  
 242 they are similar. Thus, we do not expect to be able to resolve the effects of covariates that  
 243 have similar influences on patterns in abundance and catchability (Barker et al., 2017). Given  
 244 this limitation, the most useful covariates for predictive purposes are those that either, (i) only  
 245 influence abundance or catchability, or (ii) have very different influences on abundance and  
 246 catchability. Thus, we included main and quadratic effects of trap soak time ( $E$  and  $E^2$ ), and  
 247 main and quadratic effects of temperature ( $temp$  and  $temp^2$ ) as continuous variables; we  
 248 included water turbidity ( $turb$ ) as a categorical variable with two levels (low as  $turb = 0$  and  
 249 high as  $turb = 1$ ); and we included current direction as a categorical variable with three levels

250 (current away from the lens and trap opening indicated by  $dir1 = 0$  and  $dir2 = 0$ ; current  
 251 towards the side of camera and trap indicated by  $dir1 = 1$  and  $dir2 = 0$ ; and current away  
 252 from the lens and trap mouth indicated by  $dir1 = 0$  and  $dir2 = 1$ ). We incorporated these  
 253 covariates into our chevron trap observation model as:

$$co_{s,t}^{trap} = \eta_1 E_{s,t} + \eta_2 E_{s,t}^2 + \eta_3 temp_{s,t} + \eta_4 temp_{s,t}^2 + \eta_5 turb_{s,t} + \eta_6 dir1_{s,t} + \eta_7 dir2_{s,t}. \quad (6)$$

255  
 256 In the camera catchability sub-model, we included turbidity, current direction, and main and  
 257 quadratic effects of bottom temperature as:

$$co_{s,t}^{cam} = \varphi_1 + \varphi_2 turb_{s,t} + \varphi_3 dir1_{s,t} + \varphi_4 dir2_{s,t} + \varphi_5 temp_{s,t} + \varphi_6 temp_{s,t}^2 + v_t \quad (7)$$

259  
 260 where the intercept  $\varphi_1$  allows for a systematic difference in the catchability of the camera  
 261 relative to the chevron trap. The parameter  $v_t$  is a fixed value (i.e.  $\log(1.72)$ , Bachelier and  
 262 Ballenger, 2018) that accounts for the increased field of view of the video cameras used in  
 263 2015 and 2016. All continuous covariates were centered on zero and scaled to one standard  
 264 deviation with the exception of the effort covariate. We scaled effort by subtracting 60 and  
 265 dividing by 60 to ease interpretation (effects are relevant to one hour). The absolute value of  
 266 the Pearson correlation coefficient between covariates were all  $< 0.6$  with the exception of  
 267 latitude and longitude ( $\rho = 0.87$ ); however, we chose to retain both covariates as we expected  
 268 that they would both be important for describing site-level variation in abundance and the  
 269 correlation would not impact adversely on the abundance index after model regularization.  
 270 All covariate definitions are provided in Table 1, the correlation matrix of all covariates is

271 presented in Table B1 (of Appendix B) and JAGS model code and fitting methods are  
272 provided in Appendix C.

273

## 274 *2.6 Model fitting and prior specification*

275

276 The posterior distributions of all parameters were estimated using a Gibbs sampler  
277 implemented in JAGS (Plummer, 2003). We called JAGS from program R (R Core Team,  
278 2015) using the library R2jags (Su and Yajima, 2015). All prior distributions of log-scale  
279 covariate effect parameters, including model intercepts and the fisheries index  $I_t$  were  
280 specified as diffuse normal distributions ( $N[0,100]$ ). Standard deviation parameters including  
281 all random effects were specified as scaled half Student-t distributions with input parameter  
282 values chosen to stabilize fit while inducing negligible parameter shrinkage (i.e.  $\mu = 0$ ,  $\tau =$   
283  $2.78$ ,  $k = 2$ ). Inference was drawn from 10,000 posterior samples taken from two chains of  
284  $10^6$  samples. We discarded the first 500,000 values of each chain to remove the effects of  
285 initial values and thinned the chain to every 100<sup>th</sup> value. Convergence of all models was  
286 diagnosed by visual inspection of trace plots and Gelman-Rubin statistic ( $\hat{R} \leq 1.1$  indicate  
287 model convergence, Gelman et al. 2004).

288

## 289 *2.6 Model fit evaluation and regularization*

290

291 There are two common purposes of models in applied ecology, (i) causal explanation  
292 and (ii) empirical prediction, and the same model will often not perform well for both  
293 purposes (Shmueli, 2010; Authier et al., 2016). A model used for the purpose of explanation  
294 requires that the uncertainty in parameter estimates are appropriately accounted for such that  
295 the realized 95% credible interval coverage is equivalent to the *a priori* expectation (i.e. true

296 parameter value contained within 95% CI 95% of the time). In practice, this requires that the  
297 model error structure adequately explains the residual error and, thus, can be determined with  
298 model fit tests. Alternatively, the optimal predictive model will often be a model where the  
299 covariate effect estimates are removed or shrunk towards zero through a process termed  
300 regularization (e.g. Reineking and Schroder, 2006; Hooten and Hobbs, 2015). Thus, some  
301 level of increased bias is accepted for the predictive advantage of decreased variance.  
302 Although optimal prediction of our index is our main purpose, we were also interested in the  
303 influence of our covariates on abundance and catchability. Thus, we first used a posterior-  
304 predictive check to determine an adequate error structure for our fully parameterized model  
305 for the purpose of evaluating covariate relationships (termed ‘global model’). Covariates  
306 were considered statistically different than zero when the associated 95% Bayesian credible  
307 intervals (quantile based) did not include zero. Second, for our best error structure, we used a  
308 process termed Stochastic Search Variable Selection (SSVS) to induce shrinkage of covariate  
309 effects and generate a model with optimal predictive properties to produce the fisheries index  
310 (termed ‘reduced model’). Using SSVS to produce models with desirable predictive  
311 properties was first introduced by George and McCulloch (1993) but has been thoroughly  
312 discussed in more recent ecological literature by O’Hara and Sillanpaa (2009), Tenan et al.  
313 (2014), and Hooten and Hobbs (2015).

314 We evaluated model fit of the global model for eight general model error structures  
315 with Bayesian p-values (Kéry, 2010). The Bayesian p-value is a posterior-predictive check  
316 that provides a measure of under- or over-dispersion of the data relative to the model (Kéry,  
317 2010; Hooten and Hobbs, 2015). The eight error structures were models that either included  
318 or excluded the random variables  $\varepsilon^{abun}$ ,  $\varepsilon^{trap}$ , and/or  $\varepsilon^{cam}$ . We performed our model fit  
319 evaluation by simulating our data directly from each model for each Markov Chain Monte  
320 Carlo (MCMC) iteration and calculating a Pearson residual between the simulated and

321 expected values (i.e. predicted  $\chi^2$ ) and observed and expected values (i.e. observed  $\chi^2$ ). The  
322 simulated data are considered “perfect” because they are generated directly from the model  
323 and, thus, the resulting Pearson residual represents the fit of the model when all model  
324 assumptions are perfectly met (Kéry, 2010). We then created a fit metric that is equal to zero  
325 when the Pearson residual was greater for the observed data than the simulated data and is  
326 equal to one, otherwise. The Bayesian p-value was then calculated as the mean of the  
327 posterior sample of the fit metric for each data type, where a mean of 0.5 indicates perfect  
328 model fit to the data and a mean approaching 1 or 0 indicates under- or over-dispersion of the  
329 data relative to the model, respectively.

330 We chose the procedure of SSVS to produce the reduced model and optimize  
331 prediction because preliminary analysis indicated that processing times in excess of four days  
332 may be expected for the example data. Thus, many common approaches to variable selection  
333 that either employ iterative model runs such as information theoretic methods (e.g. AIC,  
334 WAIC, DIC, etc.) or k-fold cross validation are prohibitive. Therefore, we employed SSVS  
335 which took approximately five days to complete two million MCMC iterations. We applied  
336 the SSVS method for each covariate effect parameter in Eq. 5, 6, and 8 to invoke parameter  
337 shrinkage. Specifically, we applied a hierarchical structure for each of our covariate priors  
338 that is conditional on a random effect indicator variable as:  $P(\beta_j|w_j) \sim \text{Normal}(0, \sigma_j)$ , where  
339  $\sigma_j = 100w_j + 0.01$ . The variable  $w_j$  is a random effect for each covariate that has a prior  
340 distribution of  $P(w_j) \sim \text{Bernoulli } 0.5$ , such that when  $w_j = 1$ ,  $\sigma_j = 100.01$ , approximating a  
341 standard uninformative prior on the covariate effect parameter  $\beta_j$ . Alternatively, when  $w_j =$   
342  $0$ ,  $\sigma_j = 0.01$  which approximates a highly informative prior for a  $\beta_j \cong 0$ . Thus, the  
343 conditional prior creates a region of high probability around zero similar to ridge regression  
344 or a “slab and spike” prior (Tibshirani, 1996; Ishwaran and Rao, 2005). Furthermore, the  
345 posterior mean of  $w_j$  can be interpreted as the relative support of a non-zero value of  $\beta_j$

346 similar to the posterior probabilities for different model structures obtained via reversible  
347 jump methods (e.g. Hillary 2011). However, one advantage of the SSVS process is that  
348 model predictions are automatically model averaged, providing a more refined level of  
349 regularization. Thus, we produced the index from the regularized model that included all  
350 covariates as well as the indicator variables and conditional priors.

351

## 352 2.7 Comparison of indices

353

354 To increase our insight into the value of the SSM index, we compared it to an index  
355 developed for use in the most recent stock assessment of *R. aurorubens* (Conn, 2010;  
356 SEDAR, 2018; hereafter referred to as the “Conn index”). The Conn index utilized a  
357 hierarchical analysis to combine multiple indices into a single index for use in stock  
358 assessment (Conn, 2010). The method requires prior knowledge of sampling error and  
359 constraints on process error, which may be difficult to inform. A detailed description of  
360 methods is provided in Conn (2010). In brief, the approach treats multiple, independently  
361 developed indices of abundance as measurements of the same underlying quantity (the true  
362 relative abundance), with each index subject to sampling and process error. For this  
363 application toward *R. aurorubens*, two indices were combined, one developed from video  
364 gear (Cheshire et al., 2017) and one from chevron traps (Bubley and Smart, 2017). Thus, the  
365 data were the same as those used for the SSM index, and the primary difference in  
366 methodology is that the Conn (2010) approach operates on previously created indices,  
367 whereas the approach presented here operates at the level of the observed data. By doing so,  
368 our approach more naturally accounts for the lack of independence between the gears that  
369 might be expected when sampling co-occurs (i.e., cameras are mounted on traps) and the



370 potential impact of non-independence between the sampling methods on the index  
371 uncertainty.

372 To simplify comparison of the indices we used a parametric bootstrap method to  
373 estimate the linear slope of population change through time for each index. For each year and  
374 index, we sampled 10,000 random values drawn from log-Normal distributions with the  
375 means specified as the annual index point estimates and the associated standard deviations.  
376 For each random sample, we use least square methods to estimate the intercept and slope of  
377 the index through time on the log scale. This results in a probability distribution of the log-  
378 scale linear trend for each index.

379

## 380 2.7 Model validation

381

382 To validate the efficacy of our model, we addressed two questions with a simulation  
383 experiment; (i) is our model identifiable and (ii) does it produce unbiased parameter estimates  
384 when applied to perfect data? Our methods were to define a data-generating model, simulate  
385 multiple datasets, and analyze the simulated datasets with the data-generating model. Our  
386 data-generating model is presented in Table 2 and was identical to the model described for  
387 our *R. aurorubens* analysis where the temporal abundance process is modeled as an  
388 independent variable for each year (Eq. 1, Table 2) drawn from a log Normal distribution  
389 with a mean and standard deviation set to represent observed variation in the *R. aurorubens*  
390 index. However, we excluded the random variables  $\varepsilon^{abun}$ ,  $\varepsilon^{trap}$ , and  $\varepsilon^{cam}$  to reduce the  
391 limitations of computation time. We simulated nine covariate relationships influencing sub-  
392 population level abundances, trap catchability and camera catchability ( $\theta_{1-9}$ , Table 2), where  
393 the simulated covariates,  $x_1$ - $x_9$  (Table 2) are nine separate vectors of random draws from  
394 normal distributions with mean of zero and standard deviation of one to simulate generic

395 centered and scaled covariates. We chose covariate effect sizes arbitrarily to represents  
396 different levels of effects and the absence of effects. The input values for the simulated  
397 covariate effects were,  $\theta_{1,4,7} = 1$ ,  $\theta_{2,5,8} = -0.5$ , and  $\theta_{3,6,9} = 0$ . Simulated data sets were fit  
398 with the data generating model. We report the mean absolute error as a measure of bias and,  
399 to evaluate if the credible interval coverage was appropriate, we reported when the true  
400 parameter value was excluded from the 95% credible intervals for each iteration of the  
401 simulation. All simulation code is included in Appendix D.

402

### 403 **3. Results**

404

#### 405 *3.1 Simulation study*

406

407 Our simulation study revealed that the SSM model does indeed return unbiased  
408 estimates of meta-population abundance ( $I_t$ ) and covariate relationships with appropriate  
409 credible intervals. The mean absolute error of all covariate effect estimates centered on zero  
410 (Fig. 2a) and the true value was included in the 95% Bayesian credible intervals between 91.5  
411 and 96.5% of the time. The results for the simulated relative abundance index were similar  
412 with little to no systematic bias (Fig. 2b) and 95% credible interval coverage of the true index  
413 value for 90.2 to 97.2% of simulation interactions. These results indicate that the model is  
414 identifiable and produced unbiased parameter estimates with appropriate levels of  
415 uncertainty.

416

#### 417 *3.2 Vermilion snapper analysis*

418

419 All eight error structures of the global model fit to *R. aurorubens* count data  
420 converged after  $10^6$  iterations and each required up to 96 hours of computer processing of  
421 two MCMC chains run in parallel. Our posterior-predictive check indicated that three model  
422 error structures adequately fit the data (models 1, 2, & 3 in Table 3). All of these models  
423 included a site-specific random effect in the abundance sub-model ( $\varepsilon^{abun}$ ) and either a site-  
424 specific random effect in the camera sub-model ( $\varepsilon^{cam}$ ), the trap sub-model ( $\varepsilon^{trap}$ ) or both.  
425 Global model 2 and 3 had the simplest structure of only two random effects, allowing us to  
426 exclude global model 1 as the most parsimonious error structure. Global model 3 produced a  
427 lower model deviance than global model 2 and the posterior estimates of the standard  
428 deviation of the random effect  $\varepsilon^{trap}$  were near zero when estimated with global model 1  
429 offering additional support for global model 3 as the best error structure (See Appendix E).  
430 Thus, we used global model 3 for the remaining analyses in this paper. This model included  
431 the random effects  $\varepsilon^{abun}$  and  $\varepsilon^{cam}$  and excluded the random effect  $\varepsilon^{trap}$  (Table 3).

432 Most of the covariates evaluated with global model 3 (had a statistically significant  
433 influence on abundance or catchability (Table 4). We found that the strongest determinants of  
434 sub-population abundance ( $n_{s,t}$ , equation 3) were the latitude, longitude, depth, and percent  
435 hard-bottom substrate at the sample site (Fig. 3, Table 4). However, the interaction between  
436 the latitude and longitude of the location was also a strong influencer (Fig. 3, Table 4). The  
437 only covariates of abundance that were not statistically different than zero were the main  
438 effect of depth ( $lon^2$ ,  $\beta_6 \approx 0$ , Table 4) and the bottom relief at the site ( $rel$ ,  $\beta_8 \approx 0$ , Table 4).  
439 The catchability of the chevron trap was found to be strongly related to the amount of time  
440 the trap was set ( $E$ ,  $\eta_1 > 0$ , Table 4) and its square ( $E^2$ ,  $\eta_2 < 0$ , Table 4). This relationship  
441 suggests that the number of *R. aurorubens* captured increases with trap soak time to a  
442 maximum (at ~110 minutes of soak time), beyond which the catch declines (Fig. 4a).  
443 Temperature and its square ( $temp$   $\eta_3$   $\varphi_5$  and  $temp^2$   $\eta_4$   $\varphi_6$ , Table 4) defined a pattern in

444 catchability for both the chevron trap and camera that stayed fairly constant at lower  
445 temperatures and increased rapidly at temperatures greater than  $\sim 25^\circ\text{C}$  (Fig. 4b); however,  
446 this pattern was less pronounced for the camera (Fig. 5a). Current direction influenced the  
447 catchability of both the chevron trap and camera ( $\eta_6$ ,  $\eta_7$ ,  $\varphi_2$ , and  $\varphi_3$ , Table 4) but was a  
448 stronger effect for the camera (Fig. 4c and 5c). For both gears, the lowest catchability was  
449 when the current direction was towards the mouth of the trap and camera lens, while it was  
450 the highest when the current direction was away from the trap mouth and camera lens (Fig.  
451 4c and 5c). Finally, higher levels of turbidity increased the catchability of the camera (Table  
452 4, Fig. 5b), but had no influence on chevron trap sampling efficiency (Table 4).

453 Our model regularization procedure resulted in a reduced model with the effective  
454 removal of eight covariates relative to the global model ( $w_j \ll 0.05$ , Table 4). For example,  
455 the three non-statistically significant covariates (i.e.  $\beta_6$ ,  $\beta_8$ , and  $\eta_5$ , Table 4) had  $w_j$  values  
456 equal to zero. Additionally, six statistically significant covariates (i.e.  $\beta_5$ ,  $\eta_6$ ,  $\eta_7$ ,  $\varphi_3$ ,  $\varphi_4$ , and  
457  $\varphi_5$ ) were effectively removed from the model with  $w_j$  values  $\leq 0.23$ . Although statistically  
458 different than zero in the global model, these covariates tended to have small effects sizes  
459 with relatively high levels of uncertainty (Table 4). We found that the value of several  
460 covariates with high inclusion probabilities (i.e.  $w_j \approx 1.00$ ) differed between the global and  
461 reduced model (i.e.  $\beta_1$ ,  $\beta_3$ ,  $\beta_4$ ,  $\varphi_2$ , Table 4). This is likely a result of some level of  
462 multicollinearity among covariates (particularly for latitude and longitude covariates). Our  
463 index generated from the reduced model tended to be equally precise as the index generated  
464 from the global model with an average coefficient of variation of 0.40 (range across years =  
465 0.35, 0.52) and 0.42 (range across years= 0.36, 0.51), for the reduced and global model,  
466 respectively. The observed different of 0.02 is likely not large enough to be biologically  
467 relevant.

468 Our index of *R. aurorubens* suggests high annual variation in abundance (Fig. 6a). For  
469 example, our model predicted a nine-fold increase in abundance between 1990 and 1991.  
470 After 1991, annual variation in abundance ranges between a 168% increase in 1994 and an  
471 87% decrease in 2003. This level of variation was fairly consistent across the time series (Fig.  
472 6a). The index also suggests a linear decline in *R. aurorubens* since the 1990s. A  
473 bootstrapped slope of this decline on the log scale was statistically negative ( $\mu = -0.60$ , 95%  
474 CI = -0.69, -0.51, Fig. 6b) and suggests that *R. aurorubens* are currently (2016) at about 16%  
475 of their average abundance in the early 1990s (i.e. 1990-1995).

476 The SSM index described a very similar pattern in abundance to the index generated  
477 from the methods of Conn et al. (2010); however, there were some differences (Fig. 6c). For  
478 example, the Conn index had a smaller average coefficient of variation than the SSM index  
479 (Conn = 0.35, SSM = 0.40) and demonstrated some differences in year-to-year variation in  
480 the index, however these differences were subtle (Fig. 6a, and b). Most notably, the SSM  
481 index described a stronger pattern of decline across the time frame of the data than the Conn  
482 index. The bootstrapped slope of the Conn index was statistically different than zero but  
483 nearly half the value of the SSM index ( $\mu = -0.36$ , 95% CI = -0.49, -0.24, Fig. 6d). This  
484 decline suggests that *R. aurorubens* in 2016 are at approximately 33% of their mean  
485 abundance in 1990-1995, which is over twice the value predicted by the SSM index.

486

#### 487 **4. Discussion**

488

489 We developed a state-space model that integrates data from multiple gears that are  
490 non-independent relative to the sampling process into a single fisheries index. We  
491 demonstrated its use for indexing *R. aurorubens* abundance from paired count data derived  
492 from underwater video cameras and catch data from traditional fisheries-independent baited

493 traps. The method provides a means to account for random and systematic variation in the  
494 catchability of both sampling gears and adjusts for aspects of non-proportionality due to  
495 changes in the spatial frame of sampling expected when monitoring programs are developing.  
496 The model produced unbiased estimates of meta-population level relative abundance when  
497 the model is correctly specifies and demonstrated good fitting properties. We see this  
498 modelling approach as a flexible tool that has the potential to be useful for generating  
499 fisheries indices for stock assessment for a variety of fish species sampled with paired non-  
500 independent gears, particularly traditional gears paired with underwater video cameras.

501         One of the key strengths of the SSM model is its ability to account for variation in  
502 catchability for both sampling gears. The importance of the covariates of catchability was  
503 highlighted by our SSVS model regularization procedure that indicated the optimal predictive  
504 model included many of these covariates. Furthermore, it is important to note the advantage  
505 that multiple sampling gears provide in addition to covariates when estimating parameters of  
506 state-space models. The addition of multiple gears, and thus, multiple observation sub-models  
507 to the SSM provides contrast between the residual error of each gear and the covariates that  
508 describe it. This contrast between patterns in residual error provides greater information for  
509 the model to disentangle process error from observation error. For example, when relative  
510 catch rates of the gears deviate from the expected value differently, at least one of these  
511 deviations must be due to observation error. Alternatively, when only one observation sub-  
512 model is included in the SSM, the pattern in the residual and the *a priori* choice of covariates  
513 to describe it are the only sources of information that the model has to distinguish observation  
514 error from process error. Furthermore, it is the inclusion of multiple sampling methods that  
515 allows a model that assumes independence of the index among years to be identifiable, which  
516 is a desirable option when the index will be further used to fit a stock assessment population  
517 dynamics model. With only a single observation model, a more confining structure must be

518 imposed on the index to obtain identifiability, such as a Markovian process commonly  
519 applied in state-space models (e.g. Clark and Bjornstad 2004; Jiao et al. 2008). Furthermore,  
520 greater contrast between the variation in catchability of the gears will provide the most  
521 informative data and likely result in greater index precision. Thus, the inclusion of multiple  
522 gears can be quite advantageous in this context.

523         In our case, the direction of the covariate effects on the observation sub-models  
524 tended to be consistent with previous research on the sampling efficiency of these gears  
525 (Bacheler et al., 2013b; Bacheler et al., 2013c; Coggins et al., 2014; Shertzer et al., 2015).  
526 This comes as no surprise because we based our choice of covariates, in part, on these  
527 studies. For example, we found a dome shaped relationship between trap soak time and  
528 catchability that resulted in a maximum catch at about 110 min of soak time. A similar  
529 relationship has been found for other reef fish species such as black sea bass (*Centropristis*  
530 *striata*) and is likely the result of entry and exit rates of fish into and out of the trap that  
531 change through time inversely proportional to each other (Bacheler et al., 2013c; Shertzer et  
532 al., 2015). Similarly, we found that the effect of temperature on both the trap and camera was  
533 positive with the appearance of a threshold-like response at ~25° C. Bacheler et al. (2014)  
534 found a comparable relationship between chevron trap catch of *R. aurorubens*, with a  
535 threshold at ~20° C, but did not detect this relationship for cameras. We observed a positive  
536 relationship between camera counts of *R. aurorubens* and turbidity which has also been  
537 observed for red snapper (*Lutjanus campechanus*, Coggins et al., 2014). Although this  
538 response may be counterintuitive, our data filtering process was similar to Coggins et al.  
539 (2014), which removed high turbidity data points that demonstrably impacted the counting of  
540 fish in video frames; thus, this effect may be a result of fish behavioral changes with variation  
541 in water clarity (e.g. McMahan and Holanov, 1995; De Robertis et al., 2003; Andersen et al.,  
542 2008).

543 Another important benefit of our SSM is that it can account for shifts in the sampling  
544 frame from year to year. For example, over the length of time of the Southeast Reef Fish  
545 Survey sampling program, the number of chevron traps set each year has systematically  
546 increased as the program expanded (particularly since 2011). The expanding of the program  
547 has led to changes in the distribution of traps relative to latitude, longitude, and depth (Fig.  
548 7a, b, c), resulting in variability in the mean covariate values among years with apparent  
549 systematic increases in depth and decreases in latitude over the life of the program (Fig. 7).  
550 Our model accounts for this shift by modeling the index  $I_t$  at a fixed point in space (relative  
551 to latitude and longitude) and for a fixed depth. The limitation of this method is that it only  
552 accounts for the shift in the sampling frame relative to these covariate relationships. Thus,  
553 any unaccounted for systematic spatial patterns in abundance that coincide with the  
554 expansion of sampling may still result in a biased index. This provides high incentive to  
555 determine the important drivers and structure of the spatial distribution when using this  
556 method, which could include environmental covariates as well as modeling a spatially  
557 autocorrelated residual. In our case, inspection of the residual did not reveal any non-random  
558 patterns in the spatial distribution relative to the covariates and the expanding sampling  
559 design, nor did calculating the index from only the sample locations contained within a core  
560 area that was sampled every year produce an index substantially different from the one  
561 presented in Figure 6a. These two diagnostics suggest low risk of a biased index due to  
562 shifting sampling frame, in our case (see Appendix F for details about the diagnostics).  
563 However, unaccounted for changes in the average abundance due to shifts in the sampling  
564 frame or shifts in the species distribution should be carefully considered when applying this  
565 method. This is particularly the case if the count data are derived from a fishery-dependent  
566 source, where preferential sampling that is often related to fish density is common (Pennino  
567 et al. 2018). As accounting for preferential sampling in the analysis of count data can be



568 analytically challenging (e.g. Conn et al. 2017, Pennino et al. 2018), we recommend, first,  
 569 that appropriate spatial designs be used for sampling and, when this is not possible, that  
 570 appropriate diagnostics be used to evaluate the risk of induced bias.

571

#### 572 4.1 Model extensions

573

574 There are several possible extensions to the SSM that would allow it to accommodate  
 575 various idiosyncrasies of different data sets worth discussing. One prominent extension is to  
 576 accommodate various levels of zero inflation in the sub-population model. Our example data  
 577 set was zero inflated with 75% and 70% zeros in the trap catches and camera counts,  
 578 respectively. We approximated the structural component of these zeros with the log-normal  
 579 random effect  $\varepsilon^{abun}$ ; however, this method makes explicit the assumption that these potential  
 580 zeros are actually very small non-zero values. Our model fit test suggested that this model  
 581 structure provided adequate fit to our example data; however, another option is to model a  
 582 zero-inflated spatial abundance process by including a shared Bernoulli variable in both (or  
 583 all) observation models as:

584

$$c_{s,t}^{trap} \sim \text{Poisson} \left( z_{s,t} e^{\log(n_{s,t}) + cov_{t,j}^{trap} + \varepsilon_{s,t}^{trap}} \right) \quad (8)$$

$$c_{s,t}^{cam} \sim \text{Poisson} \left( z_{s,t} e^{\log(n_{s,t}) + cov_{t,j}^{cam} + \varepsilon_{s,t}^{cam}} \right) \quad (9)$$

585

586 where  $z_{s,t}$  is a latent random variable distributed as,  $z_{s,t} \sim \text{Bernoulli}(\psi_{s,t})$ . The Bernoulli  
 587 probability of a non-zero abundance could be modeled independently for each year, as a  
 588 function of a set of spatial covariates with a logit link, or as a function of  $co \ n_{s,t}$  to create a  
 589 formal relationship between the spatial abundance and occurrence processes (e.g. Smith et al.

590 2012). Additionally, a zero-inflated observation process could be modelled by specifying  
591 unique Bernoulli processes for each observation sub-model.

592 Another prominent extension would be to model spatiotemporal variation in patterns  
593 in abundance more explicitly. For example, applying a multivariate normal prior to  $\varepsilon_{s,t}^{abun}$  to  
594 explicitly model spatial auto-correlation could be used to improve the predictive potential of  
595 the model and to better account for changes in the spatial distribution of sampling among  
596 years. Furthermore, specifying covariate effects of the spatial abundance process as random  
597 effects across years could be used to evaluate and account for non-stationarity in these  
598 relationships through time. These are only a few examples of potentially useful extensions to  
599 our model that could improve its application to various settings. Thus, we see this model as a  
600 foundation that could be easily extended to accommodate the nuances of a variety of data  
601 structures and contexts.

602

#### 603 *4.2 Management implications*

604

605 The application of our model to *R. aurorubens* revealed a systematic decline in  
606 abundance across the time period of 1990-2016. This decline was similar to, but stronger than  
607 the decline described by the Conn index (Conn et al., 2010). This discrepancy between the  
608 two indices is in the direction that would be predicted given the systematic expansion of the  
609 sampling design into latitudes, longitudes, and depths of greater abundance, and given that  
610 the Conn index does not account for this systematic expansion, while the SSM does (Figure  
611 7d). The difference also suggests that the *R. aurorubens* stock may have a lesser ability to  
612 compensate for the reductions in density due to harvest (i.e. lower productivity) than would  
613 be indicated by the Conn index. It is difficult to predict the effect this would have on  
614 management recommendations; however, we may expect the use of the SSM in a formal

615 stock assessment to result in more conservative harvest regulations to meet management  
616 targets such as Maximum Sustainable Yield (Beverton and Holt, 1957) and maintain  
617 acceptable levels of risk of overfishing (Zhou et al. 2016). Although an explicit comparison  
618 between the outcomes of formal stock assessments with each index would be necessary to  
619 know this for sure.

620

## 621 **Acknowledgements**

622

623 We thank SERFS staff members (SCDNR-MARMAP and SEAMAP-SA and  
624 NMFS/SEFSC/Beaufort) and volunteers for field assistance and the captains and crew of the  
625 NOAA Ships *Pisces* and *Nancy Foster*, R/V *Palmetto*, R/V *Sand Tiger*, and R/V *Savannah*  
626 for sampling platforms. We also thank J. Ballenger, R. Cheshire, T. Kellison, M. Reichert,  
627 and T. Smart for providing comments on earlier versions of this manuscript, as well as J.  
628 Thorson and two anonymous reviewers who's comments substantially improved this  
629 manuscript. Funding was provided by the US National Marine Fisheries Service. The use of  
630 trade, product, industry, or firm names, products, software, or models, whether commercially  
631 available or not, is for informative purposes only and does not constitute an endorsement by  
632 the US government or NOAA. The views and opinions expressed in this article are those of  
633 the authors and do not necessarily reflect the position of any government agency.

634

635

636 **References**

637

638 Andersen, M., Jacobsen, L., GrønkJÆR, P., and Skov, C. 2008. Turbidity increases  
639 behavioural diversity in northern pike, *Esox lucius* L. during early summer. Fisheries  
640 Management and Ecology 15, 5-6.

641 Authier, M., Saraux, C., and Peron, C. 2016. Variable selection and accurate predictions in  
642 habitat modelling: a shrinkage approach. Ecography 39, 1-12.

643 Bacheler, N.M., and Ballenger, J.C. 2018. Decadal-scale decline of scamp (*Mycteroperca*  
644 *phenax*) abundance along the southeast United States Atlantic coast. Fisheries Research  
645 204, 74-87.

646 Bacheler, N.M., and Carmichael, J.T. 2014. Southeast reef fish survey video index  
647 development workshop. Final Report, National Marine Fisheries Service and South  
648 Atlantic Fisheries Management Council.

649 Bacheler, N.M., Schobernd, C.M., Schobernd, Z.H., Mitchell, W.A., Berrane, D.J., Kellison,  
650 G.T., and Reichert, M.J.M. 2013a. Comparison of trap and underwater video gears for  
651 indexing reef fish presence and abundance in the southeast United States. Fisheries  
652 Research 143, 81-88.

653 Bacheler, N.M., Bartolino, V., and Reichert, M.J.M. 2013b. Influence of soak time and fish  
654 accumulation on catches of reef fishes in a multispecies trap survey. Fishery Bulletin  
655 111, 218-232.

656 Bacheler, N.M., Schobernd Z.H., Berrane, D.J., Schobernd, C.M., Mitchell, W.A., and  
657 Geraldi, N.R. 2013c. When a trap is not a trap: converging entry and exit rates and their  
658 effect on trap saturation of black sea bass (*Centropristis striata*). ICES Journal of  
659 Marine Science 70, 873-882.

660 Bacher, N.M., Berrane, D.J., Mitchell, W.A., Schobernd, C.M., Schobernd, Z.H., Teer,  
661 B.Z., Ballenger, J.C. 2014. Environmental conditions and habitat characteristics  
662 influence trap and video detection probabilities for reef fish species. Marine Ecology  
663 Progress Series 517, 1-14.

664 Barbieri M.M., and Berger J.O. 2004. Optimal predictive model selection. Annals of  
665 Statistics 32, 870–897.

666 Barker, R. J., Schofield, M. R., Link, W. A., and Sauer, J. R. 2017. On the reliability of N-  
667 mixture models for count data. Biometrika, doi:10.1111/biom.12734

668 Beverton, R. and Holt, S. 1957. On the Dynamics of Exploited Fish Populations. Chapman  
669 and Hall, London.

670 Buble, W.J. and Smart, T.I. 2017. Vermilion snapper fishery-independent index of  
671 abundance in US South Atlantic waters based on a chevron trap survey (1990-2016).  
672 SEDAR55-WP02. SEDAR, North Charleston, SC. 15 pp.

673 Campbell, M.D., Pollack, A.G., Gledhill, C.T., Switzer, T.S., and DeVries, D.A. 2015.  
674 Comparison of relative abundance indices calculated from two methods of generating  
675 video count data. Fisheries Research 170, 125-133.

676 Cao, J., Thorson, J.T., Richards, R.A., and Chen. Y. 2017. Spatiotemporal index  
677 standardization improves the stock assessment of northern shrimp in the Gulf of Maine.  
678 Canadian Journal of Fisheries and Aquatic Sciences 74, 1781-1793.

679 Cheshire, R., Bacher, N., and Shertzer, K. 2017. Standardized video counts of Southeast  
680 U.S. vermilion snapper (*Rhomboplites aurorubens*) from the Southeast Reef Fish  
681 Survey. SEDAR55-WP01. SEDAR, North Charleston, SC 21 pp.

682 Clark, J.S., and Bjornstad, O.N. 2004. Population time series: process variability, observation  
683 errors, missing values, lags, and hidden states. Ecology 85, 3140-3150.

684 Coggins, L.G, Bacheler, N.M., and Gwinn, D.C. 2014. Occupancy models for monitoring  
685 marine fish: a Bayesian hierarchical approach to model imperfect detection with a  
686 novel gear combination. *PLoS ONE* 9, e108302. doi:10.1371/journal.pone.0108301.

687 Conn, P.B. 2010. Hierarchical analysis of multiple noisy abundance indices. *Canadian*  
688 *Journal of Fisheries and Aquatic Sciences* 67, 108–120.

689 Conn, P. B. 2011. An Evaluation and Power Analysis of Fishery Independent Reef Fish  
690 Sampling in the Gulf of Mexico and U. S. South Atlantic. NOAA Tech. Memorandum  
691 NMFS-SEFSC-610.

692 Conn, P.B., Thorson, J.T., and Johnson, D.S. 2017. Confronting preferential sampling when  
693 analyzing population distributions: diagnosis and model-based triage. *Methods in*  
694 *Ecology and Evolution* 8, 1535-1546.

695 Dennis, D., Plaganyi, E., Van Putten, I., Hutton, T., and Pascoe, S. 2015. Cost benefit of  
696 fishery-independent surveys: Are they worth the money? *Marine Policy* 58, 108-115.

697 Ducharme-Barth, N.D., Shertzer, K.W., and Ahrens, R.N.M. 2018. Indices of abundance in  
698 the Gulf of Mexico reef fish complex: A comparative approach using spatial data from  
699 vessel monitoring systems. *Fisheries Research* 198, 1-13.

700 George, E.I., and McCollock, R.E. 1993. Variable selection via Gibbs sampling. *Journal of*  
701 *the American Statistical Association* 88, 881-889.

702 Gibson-Reinemer, D.K., Ickes, B.S., and Chick, J.H. 2017. Development and assessment of a  
703 new method for combining catch per unit effort data from different fish sampling gears:  
704 multigear mean standardization (MGMS). *Canadian Journal of Fisheries and Aquatic*  
705 *Sciences* 74, 8-14.

706 Gwinn, D.C., Beesley, L.S., Close, P., Gawne, B., and Davies, P.M. 2016. Imperfect  
707 detection and the determination of environmental flows for fish: challenges,  
708 implications and solutions. *Freshwater Biology* 61, 172-180.

709 Hilborn R., and Walters, C. J. 1992. Quantitative Fisheries Stock Assessment. Chapman &  
710 Hall, New York.

711 Hooten, M. B., and Hobbs, N. T. 2015. A guide to Bayesian model selection for ecologists.  
712 Ecological Monographs 85, 3-28.

713 Ishwaran, H., and Rao, J.S. 2005. Spike and slab variable selection: frequentist and Bayesian  
714 strategies. The Annals of Statistics 33, 730-773.

715 Jiao, Y., Hayes, C., and Cortes, E. 2009. Hierarchical Bayesian approach for population  
716 dynamics modelling of fish complexes without species-specific data. ICES Journal of  
717 Marine Science 66, 367-377.

718 Kimura, D.K., and D.A. Somerton. 2006. Review of statistical aspects of survey sampling for  
719 marine fisheries. Reviews in Fisheries Science 14, 245-283.

720 Kotwicki, S., Ressler, P.H., Ianelli, J.N., Punt, A.E., and Horne, J.K. 2018. Combining data  
721 from bottom trawl and acoustic surveys to estimate an index of abundance for  
722 semipelagic species. Canadian Journal of Fisheries and Aquatic Sciences 75, 60-71.

723 Langseth, B.J., Schueller, A.M., Shertzer, K.W., Craig, J.K., and Smith, J.W. 2016.  
724 Management implications of temporally and spatially varying catchability for the Gulf  
725 of Mexico menhaden fishery. Fisheries Research 181, 186-197.

726 Maunder, M.N., 2001. A general framework for integrating the standardization of catch-per-  
727 unit-of-effort into stock assessment models. Canadian Journal of Fisheries and Aquatic  
728 Sciences 58, 795–803.

729 Maunder, M.N., and Piner, K.R. 2015. Contemporary fisheries stock assessment: many issues  
730 still remain. ICES Journal of Marine Science 72, 7-18.

731 Maunder, M.N., and Punt, A.E. 2004. Standardizing catch and effort data: a review of recent  
732 approaches. Fisheries Research 70, 141-159.

733 Maunder M. N., Sibert J. R., Fonteneau A., Hampton J., Kleiber P., and Harley S. 2006.  
734 Interpreting catch-per-unit-of-effort data to assess the status of individual stocks and  
735 communities, *ICES Journal of Marine Science* 63, 1373-1385.

736 McMahon, T.E., and Holanov, S.H. 1995. Foraging success of largemouth bass at different  
737 light intensities: implications for time and depth of feeding. *Journal of Fish Biology* 46,  
738 759-767.

739 Monk J. 2013. How long should we ignore imperfect detection of species in the marine  
740 environment when modelling their distribution. *Fish and Fisheries* 15, 352–358.

741 Ntzoufras, I. 2009. *Bayesian modeling using WinBUGS*. Wiley, Hoboken, New Jersey.

742 O’Hara, R.B., and Sillanpaa, M.J. 2009. A review of Bayesian variable selection methods:  
743 what, how and which. *Bayesian Analysis* 4, 85-118.

744 Ono, K., Ianelli, J.N., McGilliard, C.R., and Punt, A.E. 2018. Integrating data from multiple  
745 surveys and accounting for spatio-temporal correlation in index the abundance of  
746 juvenile Pacific halibut in Alaska. *ICES Journal of Marine Science* 75, 572-584.

747 Parker, D., Winker, H., Bernard, A.T.F., Heyns-Veale, E.R., Langlois, T.J., Harvey, E.S., and  
748 Götz, A., 2016. Insights from baited video sampling of temperate reef fishes: how  
749 biased are angling surveys? *Fisheries Research* 179, 191–201.

750 Pennino, M.G., Paradinas, I., Illian, J.B., Muñoz, F., Bellido, J.M., López-Quílez, A., and  
751 Conesa, D. 2018. Accounting for preferential sampling in species distribution models.  
752 *Ecology and Evolution* 9, 653-663.

753 Plummer, M. 2003. “JAGS: a program for analysis of Bayesian graphical models using Gibbs  
754 sampling.” In *Proceedings of the 3<sup>rd</sup> International Workshop on Distributed Statistical  
755 computing (DSC 2003)*. March, pp. 20-22.

756 R Core Team. 2015. *R: A language and environment for statistical computing*. R Foundation  
757 for Statistical Computing, Vienna, Austria. URL <http://www.R-project.org/>.



758 Reineking, B., and Schroder, B. 2006. Constrain to perform: regularization of habitat models.  
759 Ecological Modelling 193, 675-690.

760 De Robertis, A., Ryer, C.H., Veloza, A., and Brodeur, R.D. 2003. Differential effects of  
761 turbidity on prey consumption of piscivorous and planktivorous fish. Canadian Journal  
762 of Fisheries and Aquatic Sciences 60, 1517-1526.

763 Schobernd, Z.H., Bacheler, N.M., and Conn, P.B. 2014. Examining the utility of alternative  
764 video monitoring metrics for indexing reef fish abundance. Canadian Journal of  
765 Fisheries and Aquatic Science 71, 464-471.

766 SEDAR. 2018. SEDAR 55 – South Atlantic Vermilion Snapper Assessment Report. SEDAR,  
767 North Charleston SC. 170 pp. available online at: <http://sedarweb.org/sedar-55>.

768 Shertzer, K.W., Bacheler, N.M., Coggins, L.G., and Fieberg, J. 2016. Relating trap capture to  
769 abundance: a hierarchical state-space model applied to black sea bass (*Centropristis*  
770 *striata*) ICES Journal of Marine Science 73, 512–519.

771 Shmueli, G. 2010. To explain or to predict. Statistical Science 25, 289-310.

772 Smith, A.N.H., Anderson, M.J., and Millar, R.B. 2012. Incorporation the intraspecific  
773 occupancy-abundance relationship into zero-inflated models. Ecology 93, 2526-2532.

774 Streich, M.K., Ajemian, M.J., Wetz, J.J. and Stunz, G.W. 2018. Habitat-specific performance  
775 of vertical line gear in the western Gulf of Mexico: A comparison between artificial and  
776 natural habitats using a paired video approach. Fisheries Research 204, 16-25.

777 Su, Y. and Yajima, M., 2015. R2jags: Using R to Run 'JAGS'. R package version 0.5-6.  
778 <http://CRAN.R-project.org/package=R2jags>.

779 Tenan, S., O’Hara, R.B., Hendriks, I., and Tavecchia, G. 2014. Bayesian model selection:  
780 The steepest mountain to climb. Ecological Modeling 283, 62-69.

781 Thorson, J.T., and Ward, E.J. 2014. Accounting for vessel effects when standardizing catch  
782 rates from cooperative surveys. Fisheries Research 155: 168-176.

783 Tibshirani, R. 1996. Regression shrinkage and selection via the lasso. *Journal of the Royal*  
784 *Statistical Society* 58, 267-288.

785 Walters, C.J. 2003. Folly and fantasy in the analysis of spatial catch rate data. *Canadian*  
786 *Journal of Fisheries and Aquatic Science* 60, 1433-1436.

787 Walters, C.J. and Maguire, J. 1996. Lessons for stock assessment from the northern cod  
788 collapse. *Reviews in Fish Biology and Fisheries* 6, 125-137.

789 Walters, C.J. and Martell, S.J.D. 2004. *Fisheries Ecology and Management*. Princeton  
790 University Press, Princeton, New Jersey.

791 Ward, P. 2008. Empirical estimates of historical variations in the catchability and fishing  
792 power of pelagic longline fishing gear. *Reviews in Fish Biology and Fisheries* 18, 409-  
793 426.

794 Zhou, S., Hobday, A.J., Dichmont, C.M., and Smith, A.D.M. 2016. Ecological risk  
795 assessments for the effects of fishing: a comparison and validation of PSA and SAFE.  
796 *Fisheries Research* 183, 518-529.

797

798 **Tables**

799

800 **Table 1**

801 Covariate descriptions and definitions.

802

Variable	Abbreviation	Class	Definition
Latitude	<i>lat</i>	continuous	The latitude of the sample location.
Longitude	<i>lon</i>	continuous	The longitude of the sample location.
Depth	<i>dep</i>	continuous	A continuous variable indicating the water depth at the trap location.
Soak time	<i>E</i>	continuous	A continuous variable indicating the length of time the trap was set before retrieval.
Temperature	<i>temp</i>	continuous	The water bottom temperature at the trap locations during sampling.
Turbidity	<i>turb</i>	categorical	A dummy variable indicating the level of turbidity (1 = level 2, 0 = level 1).
Substrate	<i>sub</i>	continuous	The percent of the substrate visible with the camera that is hard-bottom.
Relief	<i>rel</i>	categorical	A dummy variable with value of 1 indicating that the relief was “high”.
Current away	<i>dir1</i>	categorical	A dummy variable that is 1 when the current direction is flowing away from the camera lens.
Current side	<i>dir2</i>	categorical	A dummy variable that is 1 when the current direction is flowing perpendicular to the camera lens.

803

804

805 **Table 2**

806 Simulation structure and inputs. The equations represent the structure of the data-generating

807 model and the Inputs are the parameter values used in the simulation.

808

Data-generating model	Description	Inputs
<u>Process model</u>		
$\log I_t \sim \text{Normal } \mu, \sigma$	Temporal abundance model	$\mu = -3, \sigma = 0.93$
$\log(n_{s,t}) = \log I_t + co_{s,t}^n$	Site-level abundance model	
$co_{s,t}^n = \theta_1 x_{1,s,t} + \theta_2 x_{2,s,t} + \theta_3 x_{3,s,t}$	Spatial covariates	$\theta_1 = 1, \theta_2 = -0.5, \theta_3 = 0$
<u>Trap observation model</u>		
$c_{s,t}^{trap} \sim \text{Poisson}(e^{\log(n_{s,t}) + cov_{s,t}^{trap}})$	Trap observation model	
$co_{s,t}^{trap} = \theta_4 x_{4,s,t} + \theta_5 x_{5,s,t} + \theta_6 x_{6,s,t}$	Trap catchability covariates	$\theta_4 = 1, \theta_5 = -0.5, \theta_6 = 0$
<u>Camera observation model</u>		
$c_{s,t}^{cam} \sim \text{Poisson}(e^{\log(n_{s,t}) + cov_{s,t}^{cam}})$	Camera observation model	
$co_{s,t}^{cam} = \theta_7 x_{7,s,t} + \theta_8 x_{8,s,t} + \theta_9 x_{9,s,t}$	Camera catchability covariates	$\theta_7 = 1, \theta_8 = -0.5, \theta_9 = 0$

809

810

811

812 **Table 3**

813 Bayesian p-values for model fit evaluation. Each model includes or excludes site level  
 814 random effects in the abundance ( $\epsilon^{abun}$ ), trap ( $\epsilon^{trap}$ ), and camera ( $\epsilon^{cam}$ ) sub-models. The  
 815 Bayesian p-value is the output metric of a posterior-predictive check where a value of 0.5  
 816 indicates perfect fit of the model to the data and values approaching zero or one indicate  
 817 under- or over-dispersion of the data relative to model predictions, respectively.

818

#	Random effects included in model	Model deviance	Bayesian p-value	
			Camera	Trap
1	$\epsilon^{abun}, \epsilon^{trap}, \epsilon^{cam}$	31511.1	0.33	0.49
2	$\epsilon^{abun}, \epsilon^{trap}$	31487.2	0.11	0.67
3	$\epsilon^{abun}, \epsilon^{cam}$	31281.3	0.33	0.48
4	$\epsilon^{trap}, \epsilon^{cam}$	31741.2	0.99	0.71
5	$\epsilon^{abun}$	120003.7	0.02	0.67
6	$\epsilon^{trap}$	3081507.0	1.00	0.64
7	$\epsilon^{cam}$	183413.1	1.00	1.00
8	None	3218795.0	1.00	1.00

819

820

821 **Table 4**

822 Covariate parameter posterior summaries. Posterior means and credible intervals are derived  
 823 from posterior samples of the full model prior to model reduction. The grey text indicates  
 824 covariates that are not statistically different than zero at  $\alpha = 0.05$ . Variable definitions are  
 825 presented in Table 1. The column labeled ‘Mean (SSVS)’ is the mean of the posterior  
 826 distribution with induced shrinkage via the Stochastic Search Variable Selection procedure  
 827 (SSVS) and the column labeled ‘ $I_j$ ’ is the parameter inclusion indicator variable.

828

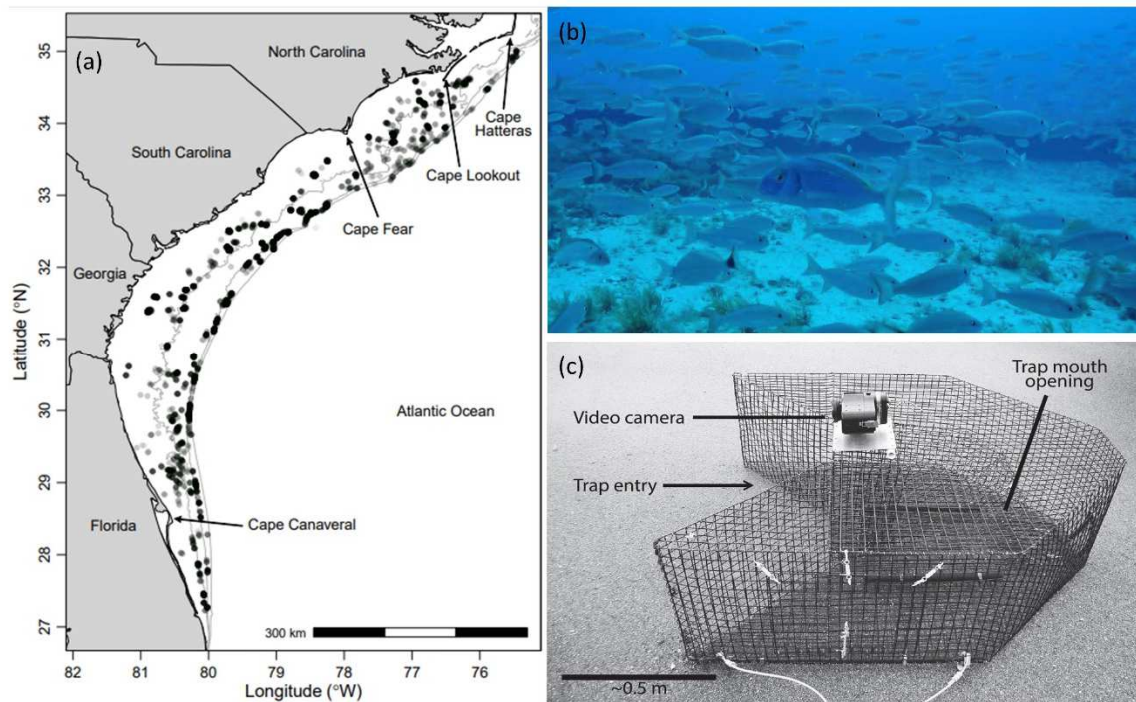
Variable	Parameter	Mean	95% Credible intervals	Mean (SSVS)	$I_j$
<u>Abundance</u>					
<i>lat</i>	$\beta_1$	-1.38	-2.03, -0.71	-1.86	1.00
<i>lat</i> <sup>2</sup>	$\beta_2$	-1.02	-1.27, -0.76	-1.00	1.00
<i>lon</i>	$\beta_3$	0.80	0.24, 1.35	1.24	1.00
<i>lon</i> <sup>2</sup>	$\beta_4$	-1.03	-1.33, -0.74	-0.64	1.00
<i>lat:lon</i>	$\beta_5$	0.79	0.29, 1.32	0.09	<b>0.12</b>
<i>dep</i>	$\beta_6$	0.12	-0.04, 0.29	0.00	0.00
<i>dep</i> <sup>2</sup>	$\beta_7$	-0.15	-0.19, -0.1	-0.14	1.00
<i>rel</i>	$\beta_8$	0.04	-0.33, 0.39	0.00	0.00
<i>sub</i>	$\beta_9$	0.61	0.50, 0.73	0.60	1.00
<u>Trap</u>					
<i>E</i>	$\eta_1$	4.65	2.86, 6.47	4.83	1.00
<i>E</i> <sup>2</sup>	$\eta_2$	-2.92	-4.28, -1.6	-3.05	1.00
<i>temp</i>	$\eta_3$	0.81	0.71, 0.91	0.72	1.00
<i>temp</i> <sup>2</sup>	$\eta_4$	0.11	0.09, 0.13	0.10	1.00
<i>turb</i>	$\eta_5$	0.04	-0.21, 0.28	0.00	0.00
<i>dir1</i>	$\eta_6$	0.63	0.32, 0.97	0.10	<b>0.23</b>
<i>dir2</i>	$\eta_7$	0.35	0.06, 0.64	0.00	0.00
<u>Camera</u>					
<i>turb</i>	$\varphi_1$	0.78	0.49, 1.03	0.79	1.00
<i>dir1</i>	$\varphi_2$	1.06	0.72, 1.43	0.59	1.00
<i>dir2</i>	$\varphi_3$	0.41	0.06, 0.76	0.00	0.00
<i>temp</i>	$\varphi_4$	0.28	0.13, 0.42	0.02	<b>0.11</b>
<i>temp</i> <sup>2</sup>	$\varphi_5$	0.05	0.00, 0.11	0.00	0.00

829

830

831 **Figures**

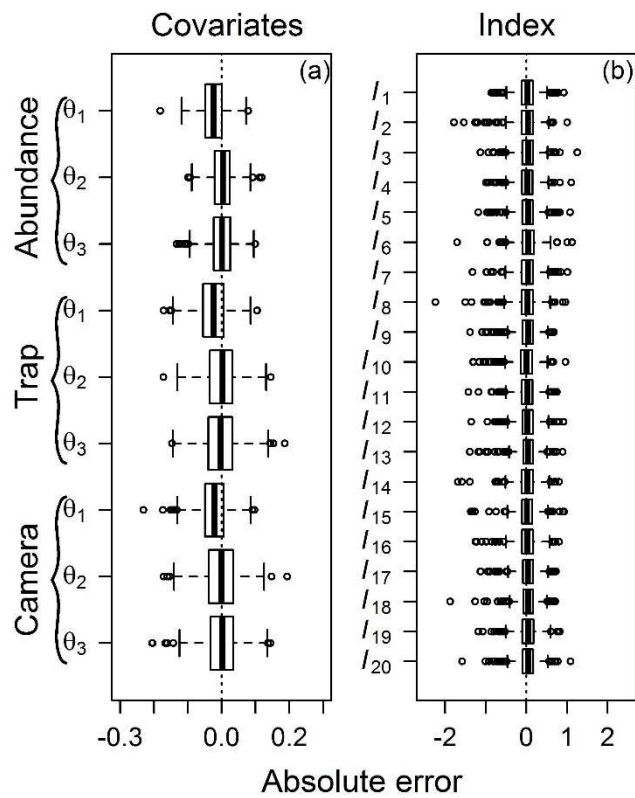
832



833

834 **Fig. 1.** Study area (a), sample video frame (b) and a Chevron fish trap outfitted with an  
835 outward-looking Canon high-definition video camera over the mouth of the trap (c). The  
836 points on panel (a) represent sample locations.

837



839

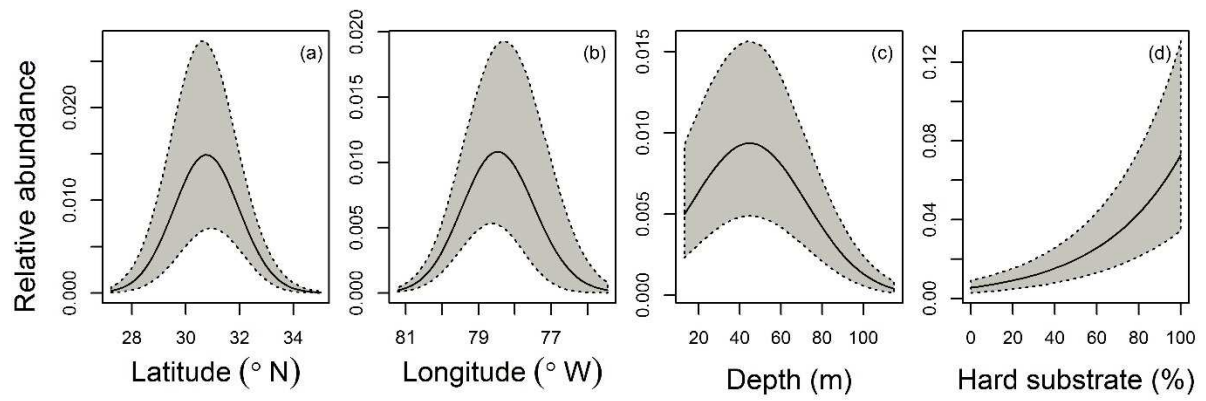
840 **Fig. 2.** The bias of simulated covariate effect parameters (a) and fishery index (b) posterior

841 distributions. Posterior samples were derived by fitting the data-generating model to 200

842 simulated 20-year data sets.

843

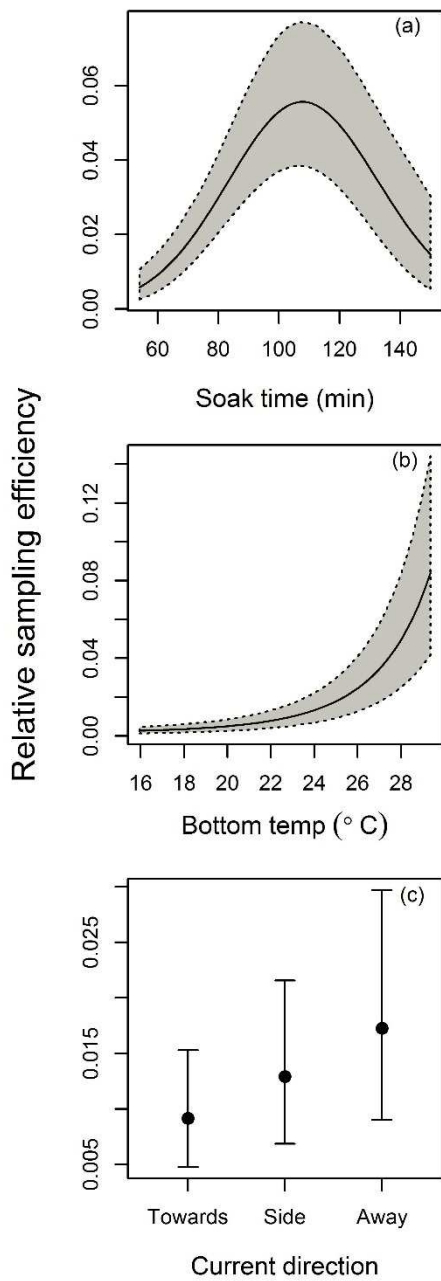




844

845 **Fig. 3.** The predicted response of sub-population abundance to spatial covariates. The grey  
 846 region represents 95% Bayesian credible intervals.

847



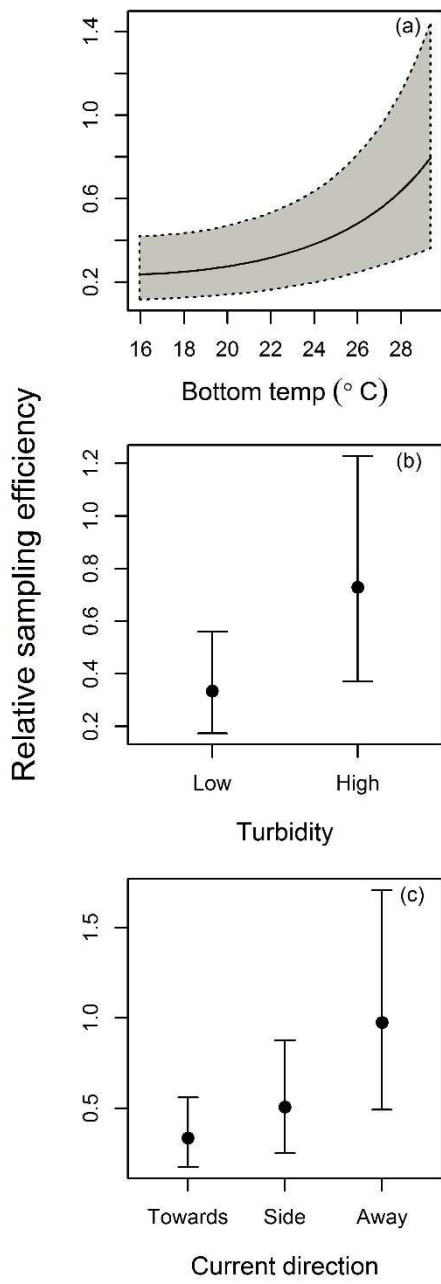
848

849

850 **Fig. 4.** The predicted response of chevron trap sampling efficiency to sampling and  
 851 environmental covariates. The grey region represents 95% Bayesian credible intervals.

852

853



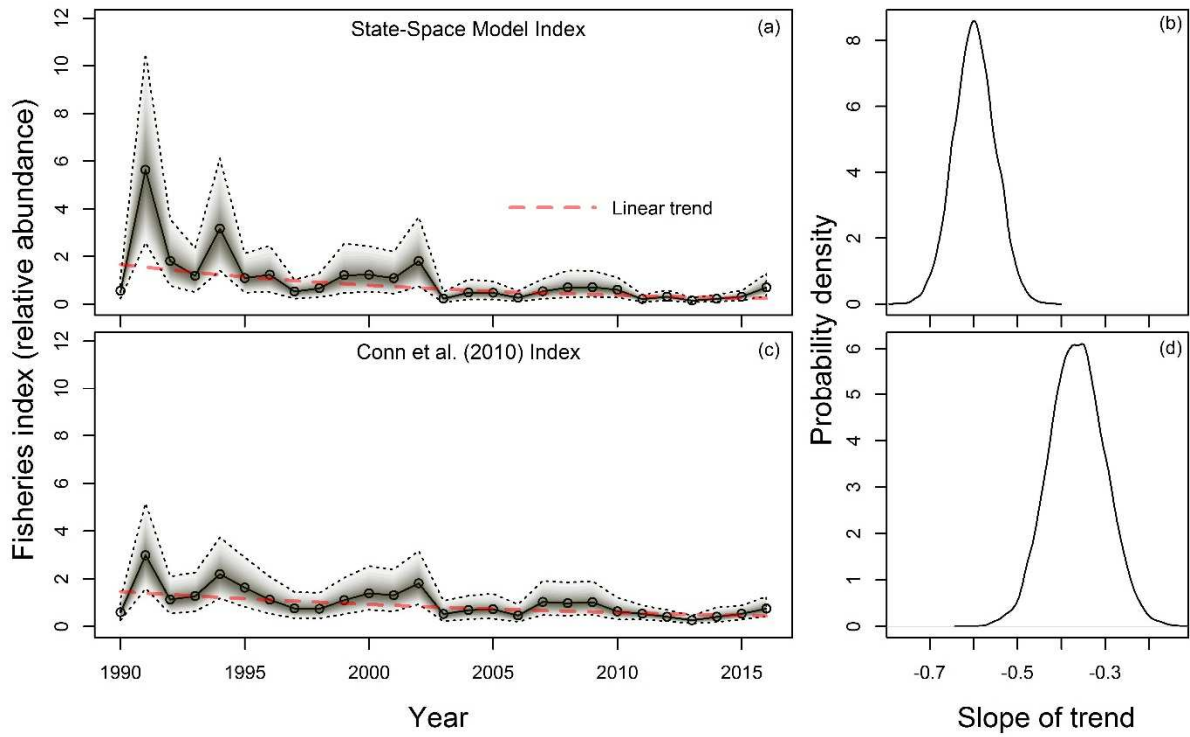
854

855

856 **Fig. 5.** The predicted response of video camera sampling efficiency to environmental

857 covariates. The grey region represents 95% Bayesian credible intervals.

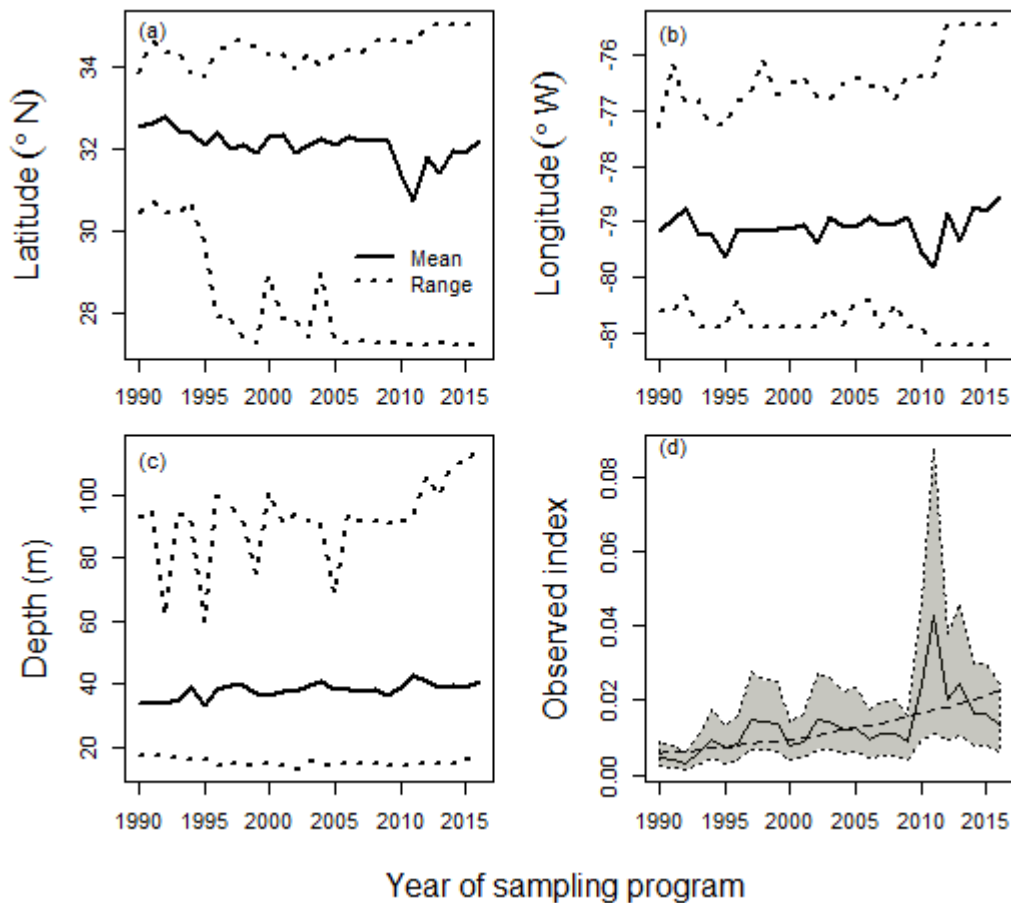
858



860

861 **Fig. 6.** The predicted annual relative abundance of the vermilion snapper meta-population  
862 using our State-Space Model (a) and the methods of Conn et al. (2010) (c). The grey region  
863 represents 95% Bayesian credible intervals. The dashed line represents the estimated linear  
864 trend. Panels (b) and (d) represent the probability distributions of the bootstrapped linear  
865 trend for each index.

866



867

868 **Fig. 7.** Impact of changing sampling frame on the predicted relative abundance at the meta-  
 869 population level. Panel (a), (b), and (c) represent the mean and range in latitude, longitude,  
 870 and depth across samples collected each year. Panel (d) is the model predicted increases to  
 871 the fishery index expected when the spatial changes on panel (a), (b), and (c) are not  
 872 accounted for. The grey region on panel (d) represents 95% Bayesian credible intervals of the  
 873 predictions and the dashed line is the log-linear trend of the predictions.

874